
AFRL-RQ-WP-TP-2016-0121

# COMPUTATIONAL AND EXPERIMENTAL EVALUATION OF A COMPLEX INLET SWIRL PATTERN GENERATION SYSTEM (POSTPRINT)

**Darius D. Sanders, Chase A. Nessler, William W. Copenhaver, Michael G. List, and Timothy J. Janczewski**

**Turbomachinery Branch**
**Turbine Engine Division**

**AUGUST 2016**



**AIR FORCE RESEARCH LABORATORY**
**AEROSPACE SYSTEMS DIRECTORATE**
**WRIGHT-PATTERSON AIR FORCE BASE, OH 45433-7541**
**AIR FORCE MATERIEL COMMAND**
**UNITED STATES AIR FORCE**

# NOTICE AND SIGNATURE PAGE

Using Government drawings, specifications, or other data included in this document for any purpose other than Government procurement does not in any way obligate the U.S. Government. The fact that the Government formulated or supplied the drawings, specifications, or other data does not license the holder or any other person or corporation; or convey any rights or permission to manufacture, use, or sell any patented invention that may relate to them.

This report was cleared for public release by the USAF 88th Air Base Wing (88 ABW) Public Affairs Office (PAO) and is available to the general public, including foreign nationals.

Copies may be obtained from the Defense Technical Information Center (DTIC) (http://www.dtic.mil).

AFRL-RQ-WP-TP-2016-0121 HAS BEEN REVIEWED AND IS APPROVED FOR PUBLICATION IN ACCORDANCE WITH ASSIGNED DISTRIBUTION STATEMENT.

*//Signature//

MICHAEL G. LIST
Program Manager
Turbomachinery Branch
Turbine Engine Division

//Signature//

ROLF SONDERGAARD, Chief
Turbomachinery Branch
Turbine Engine Division
Aerospace Systems Directorate

//Signature//

ROBERT D. HANCOCK
Principal Scientist
Turbine Engine Division

This report is published in the interest of scientific and technical information exchange and its publication does not constitute the Government's approval or disapproval of its ideas or findings.

*Disseminated copies will show "//Signature//" stamped or typed above the signature blocks.

# REPORT DOCUMENTATION PAGE

*Form Approved*
*OMB No. 0704-0188*



| 1. REPORT DATE *(DD-MM-YY)* | 2. REPORT TYPE | 3. DATES COVERED *(From - To)* |
|---|---|---|
| August 2016 | Conference Paper Postprint | 06 November 2014 – 24 June 2016 |

**4. TITLE AND SUBTITLE**
COMPUTATIONAL AND EXPERIMENTAL EVALUATION OF A COMPLEX INLET SWIRL PATTERN GENERATION SYSTEM (POSTPRINT)

**5a. CONTRACT NUMBER**
In-house

**5b. GRANT NUMBER**

**5c. PROGRAM ELEMENT NUMBER**
62203F

**6. AUTHOR(S)**
Darius D. Sanders, Chase A. Nessler, William W. Copenhaver, Michael G. List, and Timothy J. Janczewski

**5d. PROJECT NUMBER**
3066

**5e. TASK NUMBER**
N/A

**5f. WORK UNIT NUMBER**
Q1F5

**7. PERFORMING ORGANIZATION NAME(S) AND ADDRESS(ES)**
Turbomachinery Branch
Turbine Engine Division
Air Force Research Laboratory, Aerospace Systems Directorate
Wright-Patterson Air Force Base, OH 45433-7541
Air Force Materiel Command, United States Air Force

**8. PERFORMING ORGANIZATION REPORT NUMBER**
AFRL-RQ-WP-TP-2016-0121

**9. SPONSORING/MONITORING AGENCY NAME(S) AND ADDRESS(ES)**
Air Force Research Laboratory
Aerospace Systems Directorate
Wright-Patterson Air Force Base, OH 45433-7541
Air Force Materiel Command
United States Air Force

**10. SPONSORING/MONITORING AGENCY ACRONYM(S)**
AFRL/RQTT

**11. SPONSORING/MONITORING AGENCY REPORT NUMBER(S)**
AFRL-RQ-WP-TP-2016-0121

**12. DISTRIBUTION/AVAILABILITY STATEMENT**
DISTRIBUTION STATEMENT A: Approved for public release. Distribution is unlimited.

**13. SUPPLEMENTARY NOTES**
PA Case Number: 88ABW-2016-3190; Clearance Date: 29 June 2016.

This conference paper was published in the proceedings of the 52nd AIAA/SAE/ASEE Joint Propulsion Conference, Propulsion and Energy Forum, held 25 – 27 July 2016 in Salt Lake City, UT.



**14. ABSTRACT**
An assessment was conducted to determine the suitability of subscale, low-Mach-number, particle image velocimetry (PIV) testing and computational fluid dynamics (CFD) analysis to evaluate swirling flow downstream of a swirl pattern generation system composed of continuous patterns of turning vanes. Successful demonstration of the evaluation methods required acceptable comparison of the PIV and CFD to an independent five-hole probe measurement performed at the design Mach number and full-scale geometry. The focus of the investigation was on direct comparison of flow angles and flow features one diameter downstream of the swirl pattern generator. Both the subscale PIV and the CFD provide adequate representation of the swirling flow produced by the full-scale generator. The subscale PIV and CFD may be used to predict the performance of the full-scale swirl pattern generator and allow for inexpensive testing and analysis to be performed during the design process, thus improving the accuracy of generating a desired swirl pattern.

**15. SUBJECT TERMS**
swirl distortion, distortion generator, StreamVane

| 16. SECURITY CLASSIFICATION OF: | | | 17. LIMITATION OF ABSTRACT: | 18. NUMBER OF PAGES | 19a. NAME OF RESPONSIBLE PERSON (Monitor) |
|---|---|---|---|---|---|
| a. REPORT | b. ABSTRACT | c. THIS PAGE | | | Michael G. List |
| Unclassified | Unclassified | Unclassified | SAR | 25 | 19b. TELEPHONE NUMBER *(Include Area Code)* N/A |

Propulsion and Energy Forum
July 25-27, 2016, Salt Lake City, UT
52nd AIAA/SAE/ASEE Joint Propulsion Conference

# Computational and Experimental Evaluation of a Complex Inlet Swirl Pattern Generation System

Darius D. Sanders*, Chase A. Nessler†, William W. Copenhaver‡, Michael G. List*, and Timothy J. Janczewski‡
*Air Force Research Laboratory, WPAFB, OH, 45433*

**An assessment has been conducted to determine the suitability of subscale, low Mach number PIV testing and CFD analysis to evaluate swirling flow downstream of a swirl pattern generation system composed of continuous patterns of turning vanes. Successful demonstration of the evaluation methods required acceptable comparison of the PIV and CFD to an independent 5-hole probe measurement performed at the design Mach number and full scale geometry. The focus of the investigation was on direct comparison of flow angles and flow features one diameter downstream of the swirl pattern generator. Both the subscale PIV and the CFD provide adequate representation of the swirling flow produced by the full scale generator. The subscale PIV and CFD may be used to predict the performance of the full scale swirl pattern generator and allow for inexpensive testing and analysis to be performed during the design process, thus improving the accuracy of generating a desired swirl pattern.**



## I. Introduction

FUTURE aircraft designs pose critical system integration challenges to propulsion systems. The conventional approach of "podded" under-the-wing propulsion system integration is being replaced by approaches where the propulsion system is integrated into the airframe to reduce drag and improve overall air platform performance.[1] The assumptions for these designs are that the propulsion system performance will remain the same or be improved relative to conventional integration approaches. However, these non-conventional approaches produce complex flowfields at the entrance to the propulsion system. If air platform gains are to be realized, traditional propulsion system design approaches must be improved. Advances are essential in prediction of the influence of complex inlet flowfields upon compression system components, especially fans, within the propulsion system.[2] Traditionally, aircraft-propulsion integration effects have been represented by inlet total pressure distortion. However, future inlet systems will produce not only total pressure distortion but also flow angularity distortion.[3] The coupling of total pressure and flow angularity distortion poses a challenge for future aircraft designs, necessitating additional research on the generation, behavior, and impact of flow angularity.

Experimental research is required to fully understand the impact flow angularity will have on conventional fan designs and determine which design parameters need to be modified. The research must impose a broad spectrum of swirling flow features on the fan and evaluate performance changes. Based on the evaluations and the knowledge of what design features can have the greatest influence on the performance changes, it will be possible to adjust design practices to account for flow angularity.

The enabling capability to accomplish this research is the ability to easily alter inlet velocity fields at a minimal cost to the research program, in both time and funds. Many swirl generator systems have been developed to alter the flow angles upstream of a propulsion system. In most cases, the system outputs are limited to rudimentary flowfields, such as bulk swirl or twin swirl, and usually the systems are complex to implement. A new approach to swirl pattern generation, the StreamVane™, has been developed[4] to capitalize on emerging additive manufacturing capabilities to produce user-specified, complex inlet velocity fields and flow angularity.[5] Resultantly, StreamVanes offer a rapid and cost effective solution to generate complex swirl patterns with a simple device.

Prior to placing a StreamVane in front of a propulsion system, the design must be fully evaluated to establish the velocity field produced. Additional design iterations are needed if the resulting swirl pattern does not match the design intent. If subscale testing can be conducted at a lower cost, improved efficiencies in the design process can be realized. In addition to this, if the small scale testing can be conducted at lower flow rates, additional cost savings and

* Aerospace Engineer, Air Force Research Laboratory, 1950 Fifth St. WPAFB OH, AIAA Senior Member.
† Aerospace Engineer, Air Force Research Laboratory, 1950 Fifth St. WPAFB OH, AIAA Member.
‡ Principal Research Engineer, Air Force Research Laboratory, 1950 Fifth St. WPAFB OH, AIAA Fellow.

efficiencies can be had. The purpose of this investigation is to evaluate subscale StreamVane performance relative to full scale, as well as subscale performance at lower flowrates relative to the design flow rate. For this investigation, two StreamVanes were manufactured to produce the same flowfield, one at the full scale diameter of 17 inches and one at nearly 1/3 scale with a 6 inch diameter. Both experimental and CFD methods were used to quantify the scaling and Mach number effects at one duct diameter downstream of the StreamVane. 5-hole probe measurements were performed on the full scale StreamVane at the design Mach number of 0.487 and a lower Mach number of 0.15 to evaluate Mach number effects. PIV measurements quantified the performance of the subscale 6 inch StreamVane with an inlet Mach number of 0.15. Parallel to the experimental investigations, CFD analysis was conducted using the full scale geometry and executed with the design and low Mach number conditions.

## II. StreamVane™ Hardware

The StreamVane design method for swirl pattern generation was first detailed in Hoopes[4] and the design method currently has a patent request pending by Virginia Tech. A StreamVane generates a specified swirl pattern through a continuous series of changing vane profiles stacked along a number of predefined vane paths. The changing vane profiles create the necessary turning to achieve the desired swirl. The vane profile shapes are based on six-percent-thick NACA 63-series compressor-blade sections with an $A_4K_6$ meanline distribution. The series of blade shapes was specifically designed for guide-vane applications at high sub-sonic speeds (see Dunavant[6]). Test results from this blade series were detailed in Ref. 6 for cascade studies of blade solidities (chord/spacing) of 0.75, 1.00 and 1.50 at Reynolds number up to $0.3x10^6$. The test results provided relationships between lift coefficient and the turning angle produced for the blade series. Compressibility corrections were evaluated by Lieblein and Sandercock.[7] Based on the findings in Ref. 7, for the typical range of engine inlet Mach numbers the correction was found to be approximately 1°, well within the desired tolerance of the StreamVane design system. Therefore, as described in detail by Hoopes,[8] the StreamVane design method establishes a specific blade mean line from the lift coefficient relationship and the desired turning angle at specified locations. From the meanline distribution, for a fixed solidity, a vane shape is produced in the through-flow direction along a specific vane path line. The vane path lines are established as normal to the streamlines of the desired swirl profile and spaced to minimize local blockage between adjacent vanes. The current design approach does not utilize the $A_4K_6$ thickness distribution due to manufacturing complexities. Instead the design approach employs a constant thickness distribution along the defined vane meanline. A CFD-based correction from Dunavant's relationship between lift coefficient and turning was detailed by Hoopes[8] for the influence of the constant thickness vanes. The modified relationship for flat plate thickness distribution falls within that of Dunavant's for the three blade solidities evaluated.

In this investigation, two StreamVanes were designed and fabricated to produce identical swirling flow but were scaled to diameters of 6" and 17" (see Fig. 1). Both StreamVanes utilize a plastic additive manufacturing technique that is able to produce complex geometric shapes at a relatively low cost. The StreamVanes were printed using a Fused Deposition Modeling (FDM) method where layers of plastic are used to build the part along the flow direction. The base material for the 17" StreamVane was ULTEM 9085 and the print thickness was 0.010". The StreamVanes had rounded leading edges and blunt trailing edges. The 6" diameter StreamVane was an order of magnitude lower in cost than the 17" configuration due to the reduction in size and lower material costs.

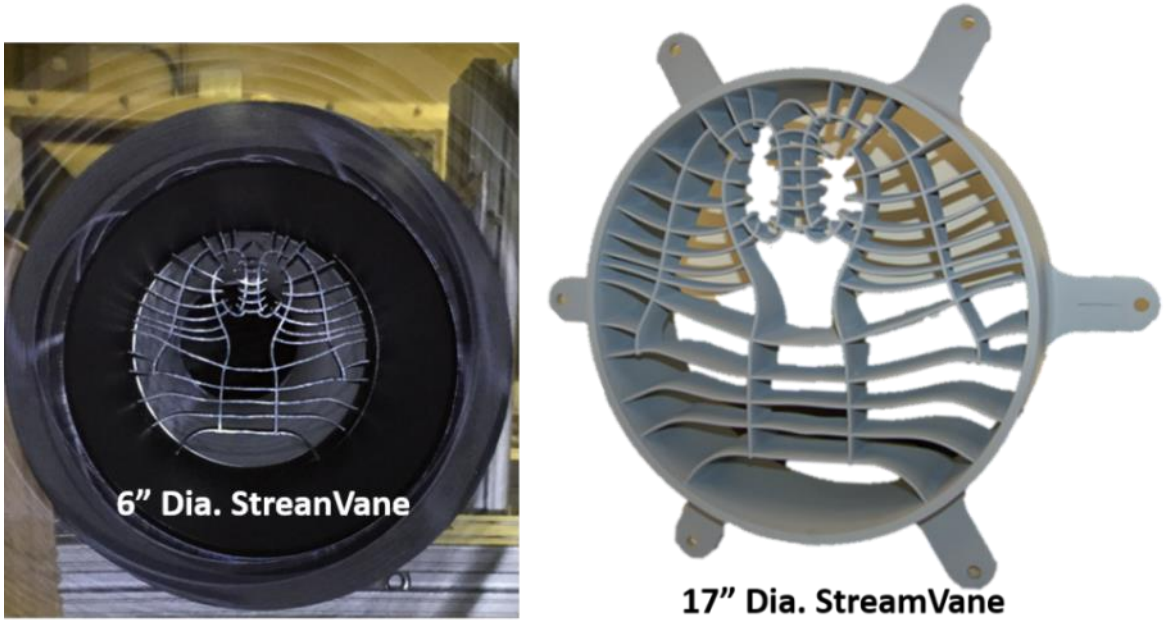


**Figure 1. StreamVane Installed in 6" Wind Tunnel and 17" Version of StreamVane**

## III. CFD Numerical Method

The desired approach to development of StreamVanes includes CFD modeling to assure the target flowfield can be produced with only one build of the final configuration, i.e., no iteration should be necessary at full scale. Demonstration that computational methods generate an accurate enough flowfield combined with subscale validation can exclude the need for full scale testing. Therefore, a computational evaluation of the performance of the StreamVane was completed to enable evaluation of the method based on experimental measurements.

The geometry was assembled and the mesh generated using the Star-CCM+ software.[9] Figure 2 shows the CFD model domain for the StreamVane geometry including the inner pipe flowpath. The inlet plane of CFD domain was placed at a length of 0.75 duct diameters from the StreamVane forward flange location, whereas the exit plane was placed 1.5 duct diameters from the aft flange location. The meshes were created using the internal mesh generator of Star-CCM+. An unstructured trimmer mesh was used due to the complex array of airfoils and support struts found in the StreamVane configuration. The trimmer mesh model consisted of hexahedral cells with the core mesh trimmed by the StreamVane surface. The trimmer mesh generator provides many desirable meshing attributes in a single meshing scheme, such as using predominantly hexahedral cells with minimal cell skewness and refinement based upon surface mesh.

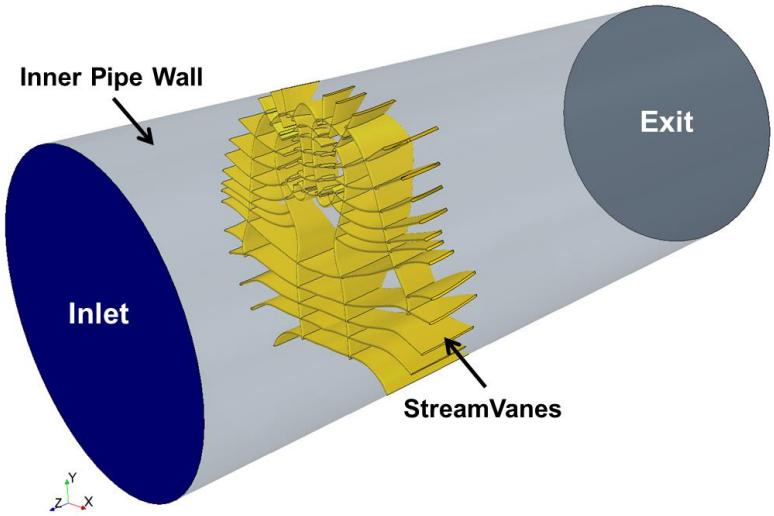


**Figure 2. StreamVane CFD Model Domain**

The trimmer mesh refinement was based on the local surface and global volume mesh size refinement controls. Growth parameters were used to control the transitioning of the mesh cell sizes from small to large at the StreamVane surface and the flowfield. A simulation using a 21.4 million cell, baseline trimmer mesh without wake refinement was executed for 2000 iterations. Additional refinement was then used

to provide spatial resolution to the wake region produced by the StreamVanes. The distribution of the turbulent kinetic energy was chosen as the parameter to define wake refinement zone. A mesh refinement function was defined to refine the mesh in an area where the turbulence kinetic energy was greater than 5.0 J/kg. The mesh was re-generated using the mesh refinement function and contained approximately 48.8 million cells. Figure 3 shows the comparison of the centerline plane of the trimmer mesh before and after wake region refinement. Prism cells were used to resolve the viscous effects from the StreamVane and inner pipe wall with a y+ range of 0.1–7 with a large number of cells in a y+ range of 2–4 and 1–3 for the inner pipe and StreamVane walls, respectively.

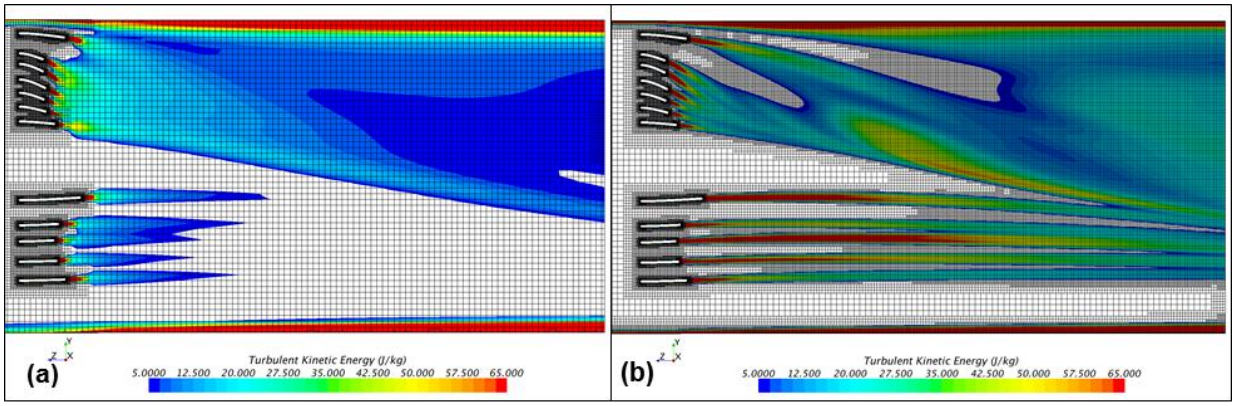


**Figure 3. Comparison of StreamVane trimmer mesh (a) before and (b) after wake region mesh refinement**

Steady RANS simulations of the StreamVane were conducted using StarCCM+ on 192 processors on a Cray XE6 system. All simulations were completed using the coupled implicit solver, which was recommended for compressible flow simulations. The steady flow solutions were initialized based on the inlet boundary conditions and grid-sequencing, executing a first-order in space, inviscid solver on successive mesh refinements. The grid sequencing provided a better approximation to the flowfield than slug flow, resulting in faster convergence of the full RANS solver. Solutions were obtained using the RANS solver with a second-order upwind spatial discretization. Flowfield convergence was considered to be achieved after residuals decreased below $10^{-5}$. Menter's k-ω(SST) turbulence model[10] was chosen due to its ability to predict fully turbulent flow resulting from adverse pressure gradients, moderate separation, and swirl dominated flow. In the simulations, a total pressure and total temperature were specified with an estimated inlet static pressure. The initial inlet turbulent viscosity ratio was set as $\mu_t/\mu = 10$ with an inlet turbulence intensity, Tu = 2%. Also, a constant exit static pressure was applied at the exit plane of the CFD domain in order to obtain the desired mass flow.

## IV. Experimental Setup

### A. Full Scale StreamVane™ 5-Hole Rake Experimental Setup

The exit flowfield from the full scale 17" StreamVane was evaluated in the Annular Cascade Facility (ACF) located at the Air Force Research Laboratory, Wright-Patterson Air Force base in Dayton Ohio. The ACF is a facility within the Compressor Aero Research Laboratory (CARL) that was commissioned in 2011. The ACF utilizes two gas turbo exhausters with a capability of over 100,000 CFM[11] to pull airflow through the annular test section. For this current investigation, the ACF was configured with a 17" diameter test section with no airfoils, and is capable of flowing over 70 lbm/s.

A 3-D CAD model of the ACF flowpath is shown in Fig. 4. The flowpath consists of flow conditioning, a bellmouth, the test section and instrumentation section, and a downstream connection to the gas turbo exhausters. Air enters the flow-conditioning barrel where it is filtered and then conditioned using a honeycomb mesh and three screens of various porosities. The airflow then enters a symmetric bellmouth where it is brought into the 17" constant diameter flowpath. Immediately downstream of the bellmouth is a removable rotator assembly that secures distortion generators in place and specifically allows for rotation of a StreamVane or other swirl distortion generator relative to the fixed flowpath. After exiting the StreamVane, the flow continues through a constant diameter spacer duct before it passes the flow measurement plane. The configuration in Fig. 4 includes the flow measurement location annotated as the Aerodynamic Interface Plane (AIP).

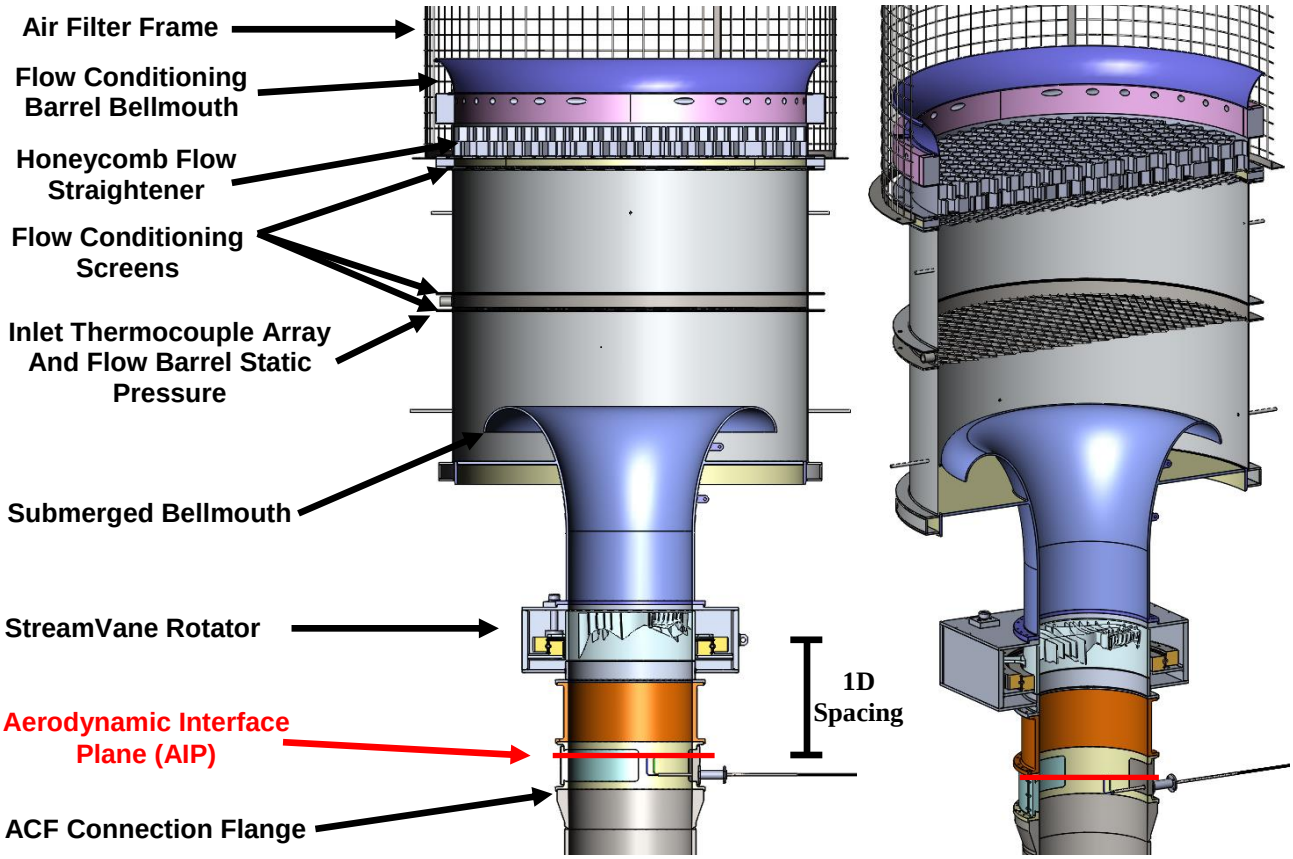


**Figure 4. Cross section of ACF flowpath layout.**

The AIP case has a constant diameter flowpath with three plugs of different sizes that can be removed to gain access to the flowpath. The plug at top dead center was modified to accept a radial traverse assembly that contained a two-element 5-hole probe rake. The AIP is the test section measurement plane and is located at the face of the 5-hole probes. The position of the AIP is one duct diameter downstream of the StreamVane mid-point. The ACF was configured to have a length of 10 duct diameters downstream of the AIP before any flowpath disturbance to assure minimal downstream influence on the measurement plane. Inlet conditions to the StreamVane were set based on the bellmouth throat Mach number. Mach number was calculated using four equally spaced throat static pressures along with the flow conditioning barrel total pressure and temperature, measured 13 inches upstream of the entrance to the bellmouth. Closed-loop feedback control of the flow rate entering the ACF was used to achieve ±0.5% Mach number control.

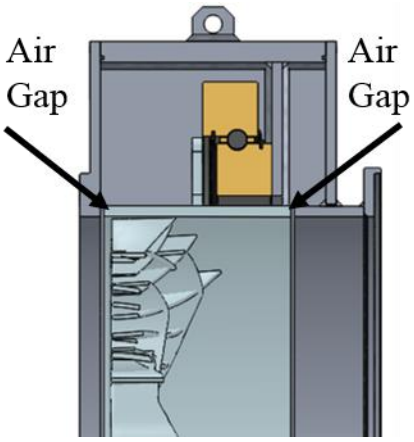


**Figure 5. Cross section of StreamVane rotator showing the location of the air gap.**

The StreamVane rotator design allows for 360-degree rotation and is accurate to less than ±0.1 degrees. Rotation was accomplished through a turntable bearing that is driven by a small electric motor. The flowpath within the rotator is continuous, except for a 1/8" gap upstream and downstream of the StreamVane to allow for rotation. The entire rotator assembly was pneumatically sealed for mass flow measurement purposes, which also minimizes the effect of the small air gap. A 3-D CAD model of the StreamVane rotator is shown Fig. 5. Rotation of the StreamVane was used here for two purposes. First, it allows for an increase in measurement density without the need for additional expensive instrumentation. The second purpose for rotating the flowfield instead of the instrumentation is that it allows for minimal invasiveness of the instrumentation to the flowfield. Typical measurement arrays used in these types of investigations include large structural supports, which can influence the flowfield and the measurement. Since this investigation was focused on measuring swirl, a single small diameter two-element 5-hole probe rake was preferred over the typical large rake bodies that could have a potential effect at low Mach number.

### B. Two-Element 5-Hole Probe Rake

A two-element 5-hole probe rake was developed to measure time-averaged swirl at the ACF test section measurement plane. The traversing rake, shown in Fig. 6, was designed in-house and contains two 5-hole probes developed and calibrated by AeroProbe Inc. The two calibrated AeroProbe 5-hole probes were assembled into a single 3/8 inch diameter, 19 inch long, cylindrical rake that can be remotely traversed radially at the AIP.

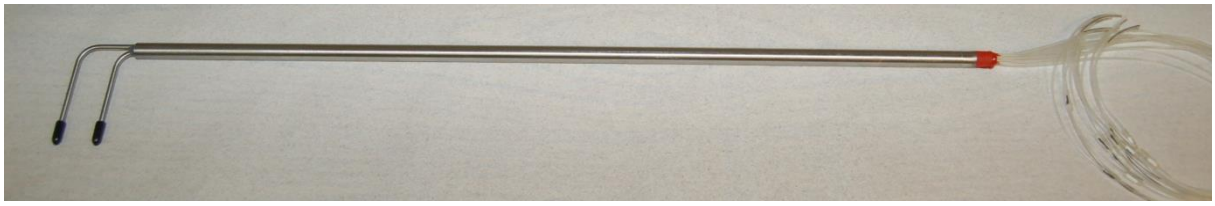

**Figure 6. Two-element, 5-hole probe rake.**

The spacing of the two probes relative to each other was chosen to match the outer probe spacing of the SAE S-16 recommended 40-element probe positions with probe radii at centers of equal area.[12] In this orientation, when the traversing rake is inserted to the zero insertion position, Probe # 1 is located 0.435 inches from the wall with 0.952 inches between the two probes. Control of the radial positioning of the probes was attained through use of a Rotodata radial traverse system (see Fig. 7). The traverse was attached onto a plug designed for installation into the AIP case top dead center window slot. This traversing capability coupled with the StreamVane rotation was used to improve data resolution in regions of high velocity gradient.

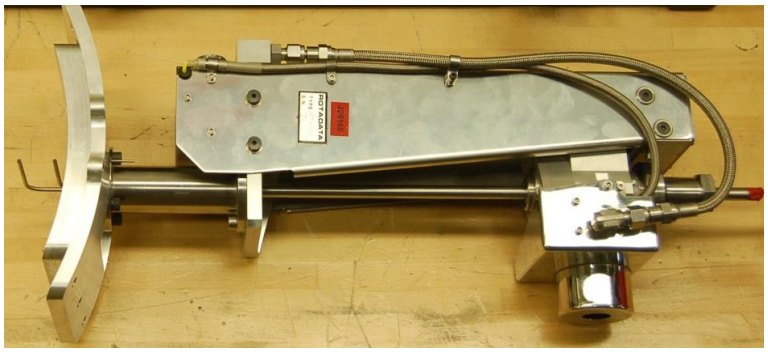

**Figure 7. 5-Hole probe rake installed in traverse and mounted to AIP window plug.**

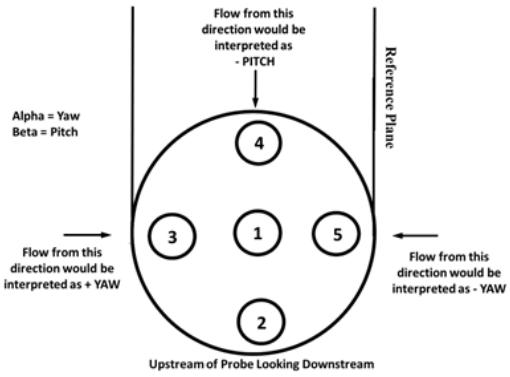


**Figure 8. 5-Hole probe measurement port orientation.**

The two 5-hole probes were manufactured and calibrated individually by AeroProbe and shipped to AFRL for assembly. Calibration data used for this research program included pitch and yaw at angles ranging from ±50° and ±38° respectively, at flow Mach numbers 0.3, 0.4, 0.5 and 0.6. Figure 8 shows the orientation of the probe face relative to the pitch and yaw directions along with the sign convention used for this investigation.

The data collected was processed using a method based upon the work of Lee and Wood[13] and Paul, et al.[14] The original methods broke the pitch-yaw space of the probe into various regions based upon the differences between pairs of holes. This was made more robust by including additional overlaps in the regions to eliminate the potential for hysteresis. An iterative technique for determining the appropriate Mach number and performing calibration table interpolation was developed to provide the final flow angle result.

### C. Subscale StreamVane™ Time-Averaged 3-D PIV Experimental Setup

The 6" StreamVane was positioned at the exit of the low speed wind tunnel at the Virginia Tech Turbomachinery and Propulsion Laboratory. The tunnel flow is generated by a constant speed 15 HP motor connected to an Aerovent Model 630 BIA centrifugal blower. The blower is rated at 12,000 CFM at a delivery pressure of 8 inches of water. Design details are provided by Tkacik.[15] The maximum flow rate produced by the centrifugal blower was selected. A schematic of the tunnel is shown in Fig. 9 (see Ref. 16). The tunnel freestream flow conditions were established from PIV measurements at clean conditions. Tunnel upstream velocity for the StreamVane study was 162 ± 3 ft/s.

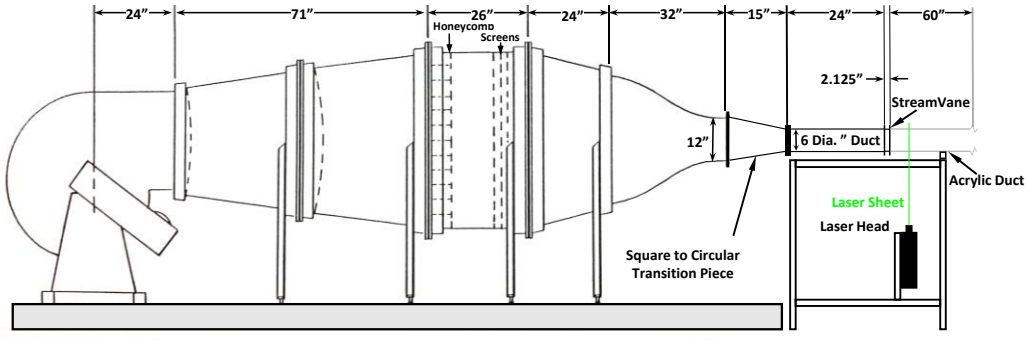


**Figure 9. Schematic of Virginia Tech 6" Wind Tunnel**

The software utilized to control the experiment and process the data is LaVision DaVis version 8.3.0 with a stereo package included. The cameras were LaVision Image Pro4X with 2048 x 2048 pixels resolution. The laser was a Quantel PIV systems Nd:YAG rated for 200 mJ/pulse. The optics used to create the laser sheet were a LaVision collimator and a -10 mm cylindrical lens. The time delay between images was 18 $\mu$s, and the data was acquired at a laser pulse rate of 4 Hz. The viewing image size was set at approximately 6.3" to obtain full AIP measurements and resulting in a resolution of 330 pixels/in. The maximum through-flow velocity level is nominally 165 ft/sec. The expected particle maximum travel between images is approximately six pixels, which is adequate to acquire acceptable correlations of particle travel. In addition, since this is stereo PIV the sheet thickness must be considered relative to the delay setting. In Ref. 17, it was recommended that the out of plane displacement of the particles should not exceed 30% of the light sheet thickness. For this experiment, and the delay setting of 18 μs, the out-of-plane displacement is 0.035 in (0.9 mm). The laser sheet thickness is approximately 0.12 in (3 mm); therefore, this criterion is also met. The seed material was sub-micron in size and introduced upstream of the wind tunnel blower with a Concept Engineering Ltd, Colt 4 seeder. Figure 10 shows the overall data acquisition configuration.

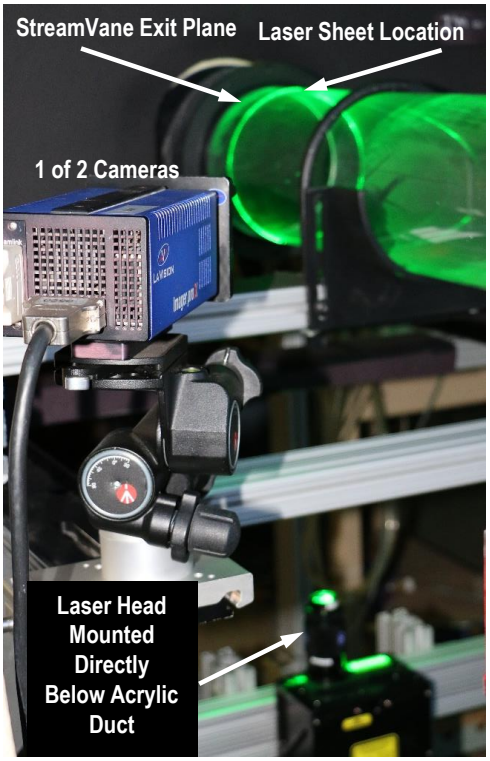


**Figure 10. PIV Experimental Configuration.**

## V. Results

Results of CFD simulations, subscale PIV, and 5-hole probe data are discussed and compared. The CFD and 5-hole probe investigations were conducted at the design Mach number of 0.487 and at an off-design Mach number of 0.15. The subscale PIV data was only collected at the off-design Mach number of 0.15.

### A. CFD Analysis

The CFD model of the StreamVane full scale geometry was simulated at two different AIP Mach Number conditions for comparison with experimental results. The contours of the swirl angle for the full pattern CFD one duct diameter downstream are shown in Fig. 11. The magnitude of swirl was normalized with respect to the maximum absolute value of the swirl from the 5-hole probe dataset at the design Mach number. The in-plane velocity vectors were super-imposed to the swirl angle contours to show the behavior of the velocity field. The CFD predicted a symmetric swirl profile with a group of four vortices located closer to the duct centerline and two vortices near the sides.

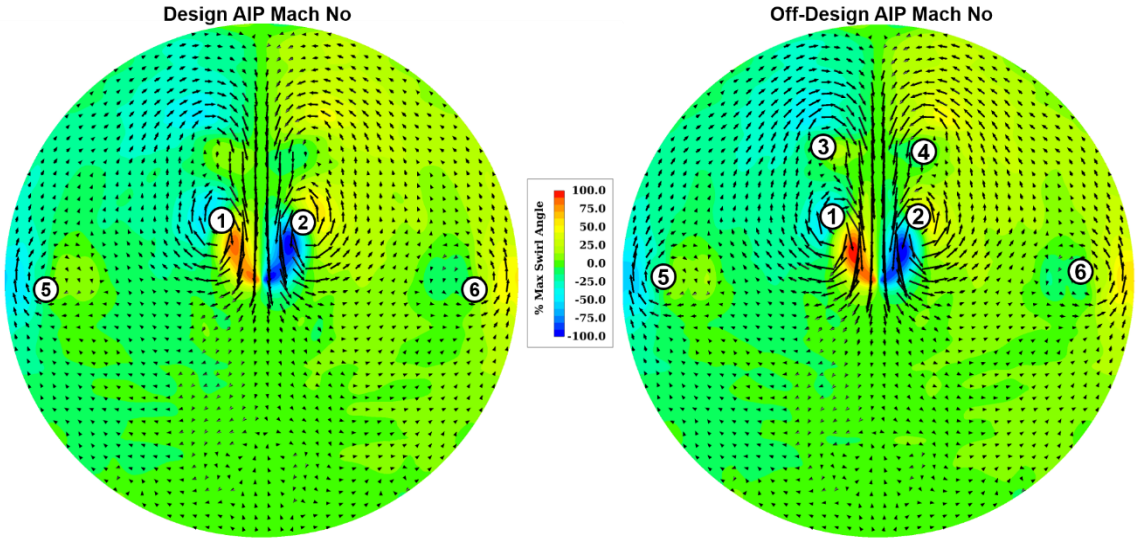


**Figure 11. CFD Contours of the Swirl Angle at Off-design and Design Mach Number.**

Figure 12 shows a focused view of the group of vortices located in the center of the duct for both CFD cases. Streamlines were included to visualize the localized flowfield behavior of the swirling flow structures produced by the StreamVane. The CFD shows, in the off-design case, four vortices symmetric about the duct centerline labeled (1)-(4) which consisted of one large single vortex (Vortex (2) & (3)) and a smaller weaker vortex above it (Vortex (1) & (4)). For the design Mach number case, the higher velocity flow has caused the four vortices to merge into two symmetric vortices.

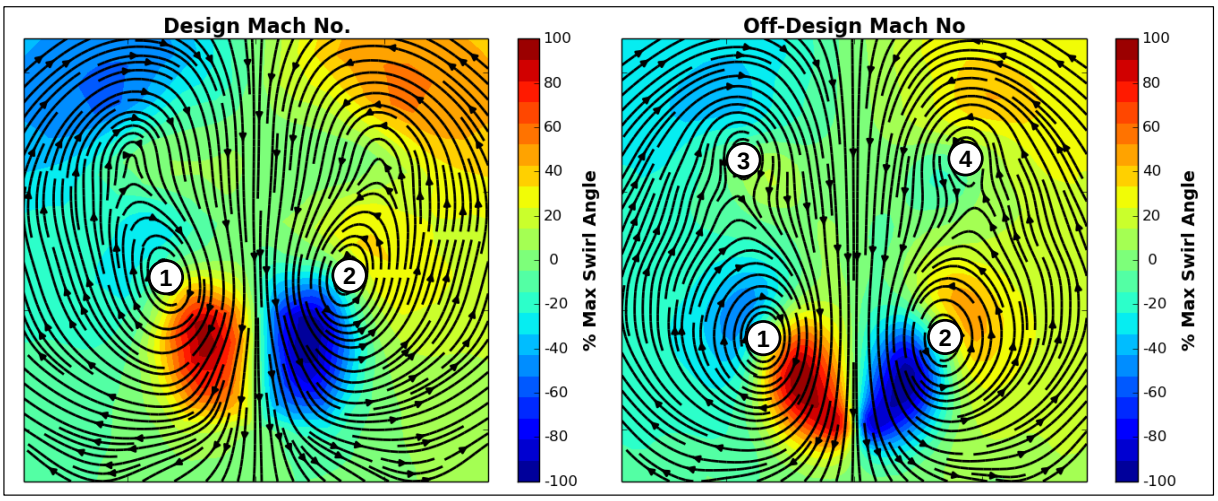


**Figure 12. Mach Number Comparison of Focused View of Swirl Angle Contours with Flowfield Streamlines**

The unique pattern of total pressure recovery contours in Fig. 13 was due to wakes produced by the StreamVane airfoils and support struts. The area average total pressure recovery was 0.998 and 0.978 for the off-design and design CFD cases, respectively. As expected, the design case had the lowest recovery due to the increased viscous losses associated with the StreamVane wakes.

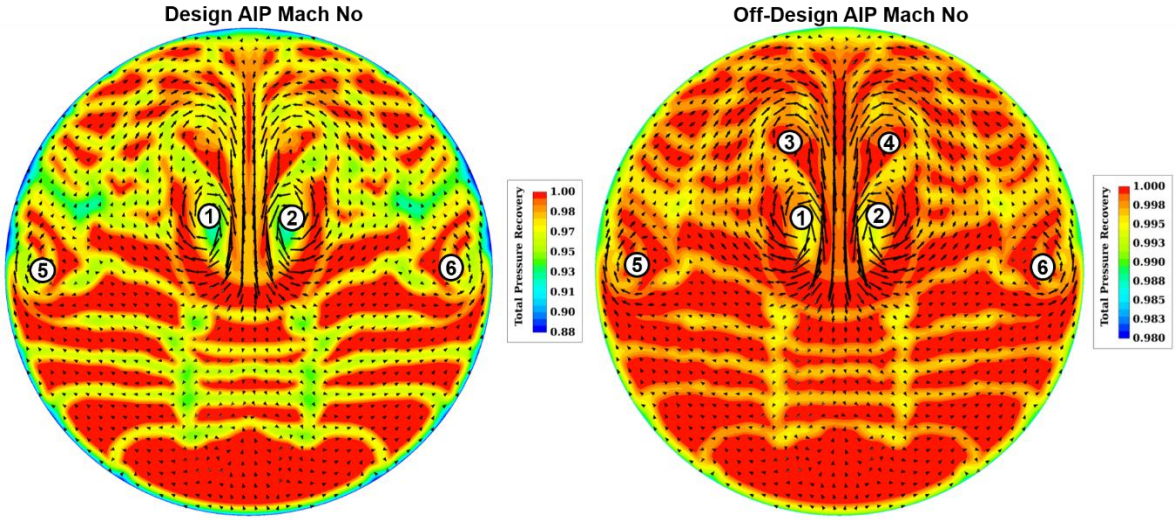


**Figure 13. CFD contours of the Total Pressure Recovery at off-design and design AIP Mach numbers.**

### B. Full Scale StreamVane™ 5-Hole Rake Analysis

The exit flowfield of the 17" StreamVane was interrogated with a two-element 5-hole probe rake located one duct diameter downstream of the StreamVane midpoint. The measurement grid used to characterize the exit flowfield was chosen based on the size and location of the flow features the StreamVane was designed to create. As mentioned previously, the 5-hole probe rake was mounted on a radial traverse allowing multiple radial positions to be measured. Additionally, the StreamVane was also rotated relative to the 5-hole probe rake, allowing detailed measurements to be made throughout the non-uniform flowfield. Figure 14 shows the measurement locations used for the 5-hole probe rake. All figures presented are viewed as upstream looking downstream at the AIP.

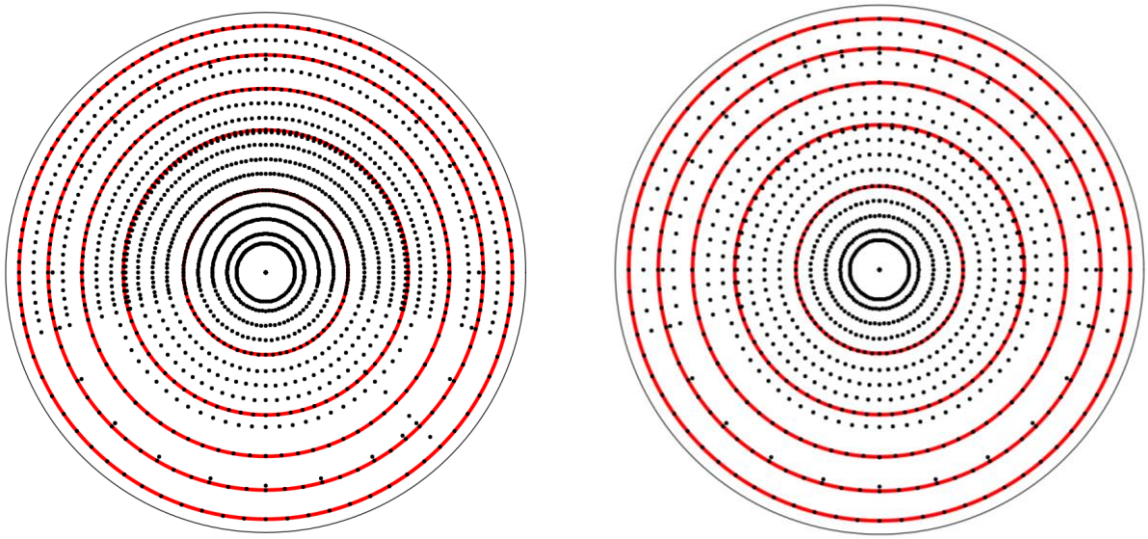

**Figure 14. 5-Hole probe rake measurement locations. Left: Design Mach condition, Right: Off-design condition. Red circles indicate percent spans of 31.6%, 54.8%, 70.7%, 83.7%, and 94.9%.**

For the two Mach numbers tested, two different non-uniform measurement grids were used to quantify the exit flowfield. Particular interest was placed around the top 210-degree sector, where most of the flow features of interest

lie. For the design condition a dense measurement grid was used to fully quantify the flow features of interest. For this condition, 17 unique radii were measured along a circumference from 255 degrees to 105 degrees, in 2.5-degree increments. Outside of this circumferential sector, radial positions were down selected to 13 radii and rotations were increased to 5-degree increments. In total there were 1,822 measurement points used to quantify the exit flowfield at the design Mach number. Similarly, for the off-design condition the same 17 unique radii were measured along a circumference from 255 degrees to 105 degrees, in 5-degree increments. Outside of this circumferential sector, the same 13 radial positions were measured also in 5-degree increments for a total of 1,108 measurement points. Five of the 17 radial positions were located at centers of equal area (red rings) for comparison to previous data sets. The resulting measurement grids were based on an optimization to acquire the data needed to resolve flow features of interest while minimizing the time required running the experiment.

In an effort to increase the repeatability of the measurements, each measurement was made using a running average of the measured pressure value. Since the 5-hole probe rake measures steady state pressure, using a running average of the measured pressure allows for improved accuracy when measuring a semi-unsteady flowfield. A total of 150 measurements were used in the running average calculation for a single data point. This resulted in a 60 second settling time for each traverse position.

Repeatability of the measurements (and post processing method) was verified through acquisition of velocity field data for 72 common traversing probe locations, where probe #1 and probe #2 were placed at a common radial location. The data sets spanned different test days, includes data from the two Mach number conditions, and the full range of the AIP circumference. From this comparison, the probe to probe error for common boundary conditions was determined. From these repeatability studies, the 5-hole measurements are repeatable to within ±6% of the peak swirl angle; the total pressures within ± 0.016 psi, static pressures within ±0.046 psi, and finally the measured AIP Mach number is nominally repeatable to ±0.5%.

From the five individual pressure measurements at each location, plots of total pressure and flow angle including the swirl angle are presented. Side to side comparisons of the two Mach numbers are made in each figure. All plots were non-dimensionalized to the maximum value of swirl angle. Black rings were placed around the contours to indicate the flowpath wall.

The total pressure measured one duct diameter downstream of the StreamVane midpoint is shown in Fig. 15 for both Mach numbers. A uniform pressure profile is desired so the effects of swirl are isolated from pressure distortions. The total pressure recovery is 0.969 at design Mach number and 0.997 for off-design Mach number. The localized regions with lower levels of loss are evident throughout the flowfield and align with open StreamVane passages where blockage is minimal.

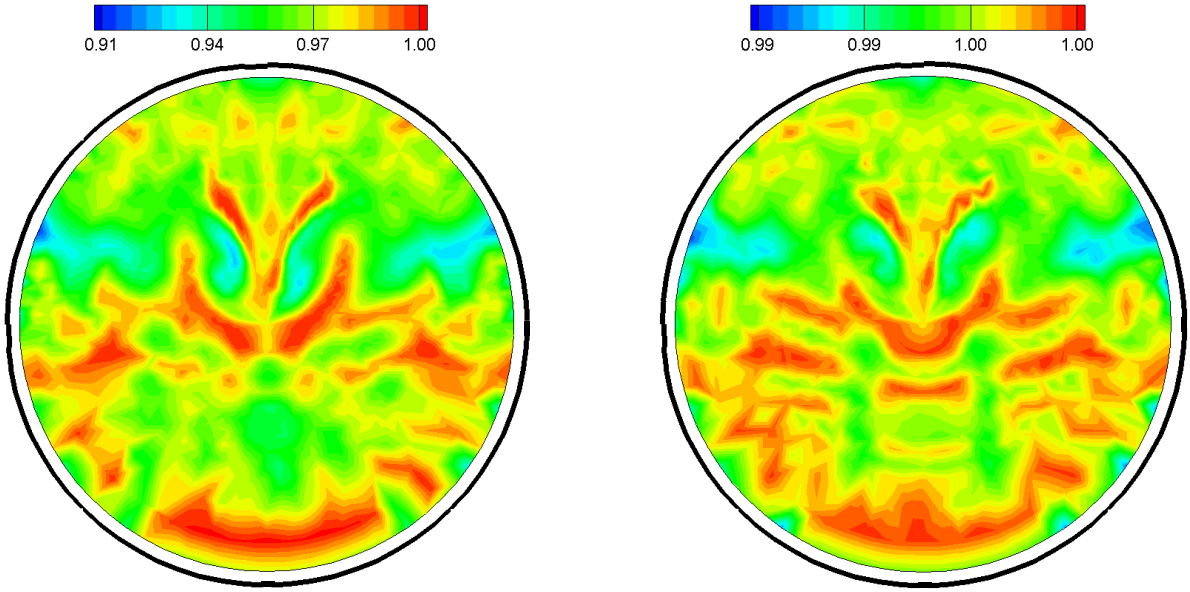


**a) Design Mach Number** **b) Off-design Mach Number**

**Figure 15. Total pressure contours normalized at the AIP for both Mach numbers.**

Combining the pressures measured by the 5-hole probe, a flow vector can be calculated for each measurement location based on the calibration data. Figure 16 shows the vector field, scaled to the maximum throughflow velocity, for both Mach numbers tested superimposed upon the normalized swirl angle. As mentioned previously, measurement resolution was increased for the design Mach number to fully resolve the details of the flowfield.

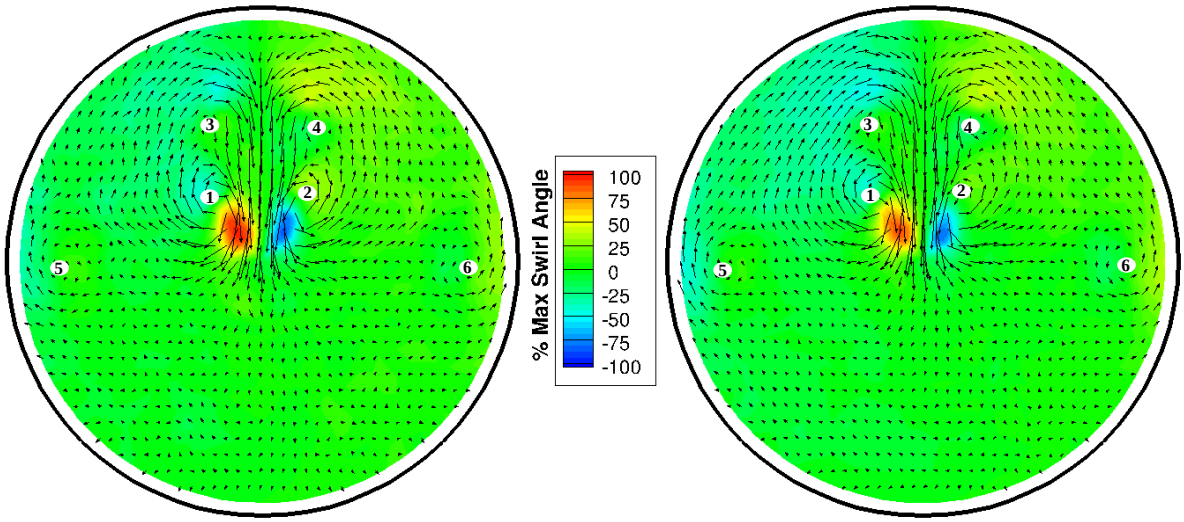


**a) Design Mach Number** **b) Off-design Mach Number**

**Figure 16. Comparison of AIP measured vector field for both Mach numbers with contours of swirl.**

There are six main flow features of interest generated by this StreamVane design and they are highlighted and numbered in Fig. 16 for both Mach numbers tested. Features one through four are regions of tight vortices, all interacting with each other. Features numbers one and two have the greatest extent of swirling flow and are counter rotating relative to one another. Flow features numbered three and four are just on top of features one and two and are also counter rotating relative to each other and in the same direction of rotation as features one and two respectively. The same is true for features five and six, which are also counter rotating relative to each other and in the same direction as their neighbors.

Qualitatively, the unique swirl pattern generated at the design Mach number matches the pattern generated at the low Mach number condition. In order to quantify the extent to which the low Mach number condition varies from the design condition, comparisons need to be made that look at the size and the location of the flow features generated. Since variations are expected, a simple subtraction of the two vector fields would be an unrealistic comparison that would not include an acceptable tolerance. Alternatively, looking at swirl magnitude across the circumference at various radial locations, accounting for measurement repeatability, enabled qualitative comparisons. Any Mach number effects on swirl would then be indicated as differences in the line plots. If the location, size, and extent of the flow features match, then the line plots would fall on top of each other.

Since the pattern is nearly symmetric, the centers of rotation of the six vortices approximately fall on three unique radial positions. Figure 17 contains three line plots of swirl magnitude versus circumferential position for three radial positions nearest the centers of rotation. All three plots have a unique shape that is a function of the flow features and their locations. Not only is the shape of the plots matched for the low Mach number condition but magnitude also falls within the measurement repeatability for most circumferential positions. Based upon the close match the Mach number range does not have large effects on the swirl magnitude, location, or size of the flow features generated by this StreamVane.

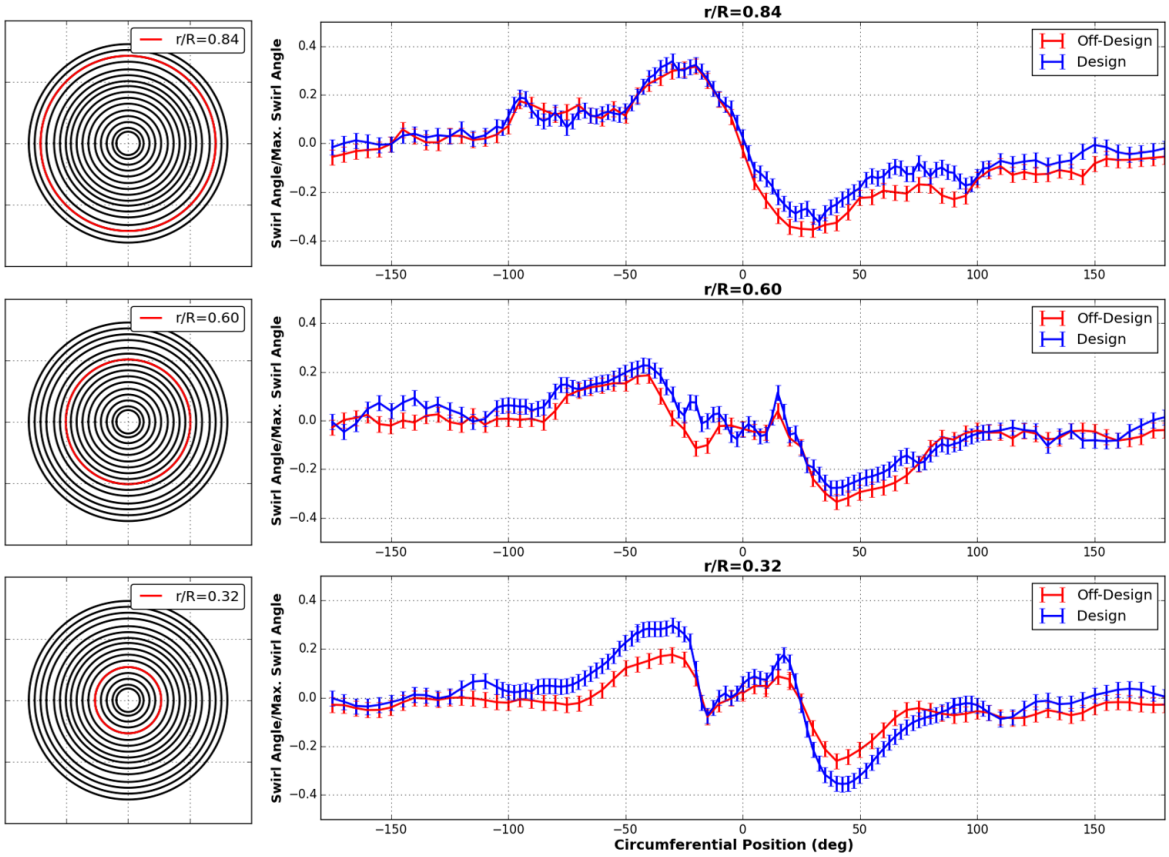


**Figure 17. Line plot of swirl magnitude vs. circumferential position for three radial positions**

### C. Subscale StreamVane™ Time-Averaged 3-D PIV Analysis

The exit flowfield of the 6" StreamVane was evaluated through 3-D Particle Image Velocimetry (3D-PIV) at one diameter downstream of the StreamVane midpoint. The 3D-PIV data was processed in windows of 64x64 pixels using two reduction passes at this resolution with a 50% overlap, resulting in velocity field information reported at a 2.4 mm resolution. Figure 18 shows the resolution of the data acquired.

No data interpolation or filtering was used with the DaVis analysis package. The data was filtered using MatLab routines to remove erroneous vectors, based on magnitude and data variance criteria. No vector substitution or interpolation was utilized in creating the measured velocity profiles. The RMS error based on experimental setup is 11.25% and 8.75% for radial and swirl angle are respectively. In addition, the experimental errors in circumferential position of vortices is 3 degrees, and radial position 2.6% of the span. Details of how these errors were derived are provided in the appendix.

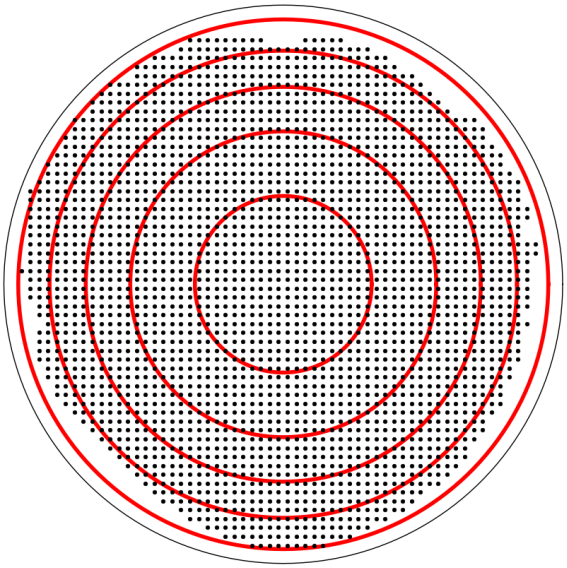

**Figure 18. 3D-PIV Measurement Resolution.**

The complete swirl angle field measured with the PIV system is shown in Fig. 19. In general, 6 discrete swirling flow features can be seen. The swirling flow features match those seen in the CFD and 5-hole probe data. The out-of-plane velocity field measured from the 3D-PIV is also shown in Fig. 19. The wakes from the individual StreamVanes are evident with the presence of viscous mixing. Although total pressure is not captured by PIV, the velocity deficit is consistent with the wake deficits seen in the total pressure contours for the CFD and 5-hole probe.

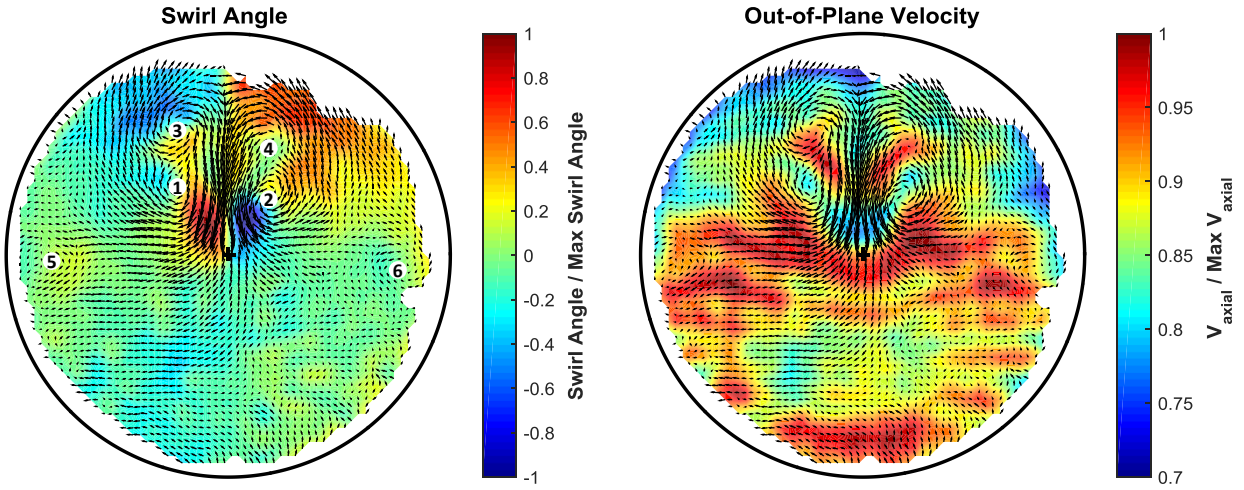


**Figure 19. 6" StreamVane Swirl Angle and Out-of-Plane Velocity Field.**

### D. Comparison to the Full Scale StreamVane™ Exit Flowfield

The PIV and CFD were compared to the 5-hole probe data to assess the ability of the methods to capture the flowfield and to determine if Mach number or scaling effects were present in the subscale PIV. To assess the ability to capture the flowfield, subtraction of the datasets was used to produce a percent difference. The percent difference indicates both location and error amount. Line plots were used to assess Mach number and scaling effects. In investigating Mach and scaling effects, the 5-hole probe measurements of the 17" StreamVane were considered the true exit flowfield. The assessment focused on the ability of PIV and CFD methods to capture the pertinent swirling flows and the ability of the CFD to predict total pressure field.

Subtraction of the different datasets was accomplished by interpolating to the 5-hole probe points and performing a direct difference. The Clough-Tocher method[18] was used to produce a piecewise cubic, C1 smooth interpolant of the PIV and CFD flowfields. Next, the probe locations from the 5-hole dataset were used to produce interpolated PIV and CFD values. Finally, the interpolated PIV and CFD values were subtracted from the 5-hole probe data.

The flowfield values of interest were subtracted to determine a percent difference between the assumed true value and the PIV or CFD methods. The swirl angle comparison shows that the swirling flow is largely similar between the three datasets. Contours of swirl angle and contours of the percent difference between the PIV and CFD relative to the 5-hole data are shown in Fig. 20 for the design Mach number case. The region of interest is highlighted with a black box. The pair of swirling flow features is visible near top dead center and within the box as regions of high magnitude. The peak values of swirl represent a stronger swirling flow region near the center of the flowfield. The higher magnitude percent difference contours represent differences in the shape and magnitude of the swirling flow features.

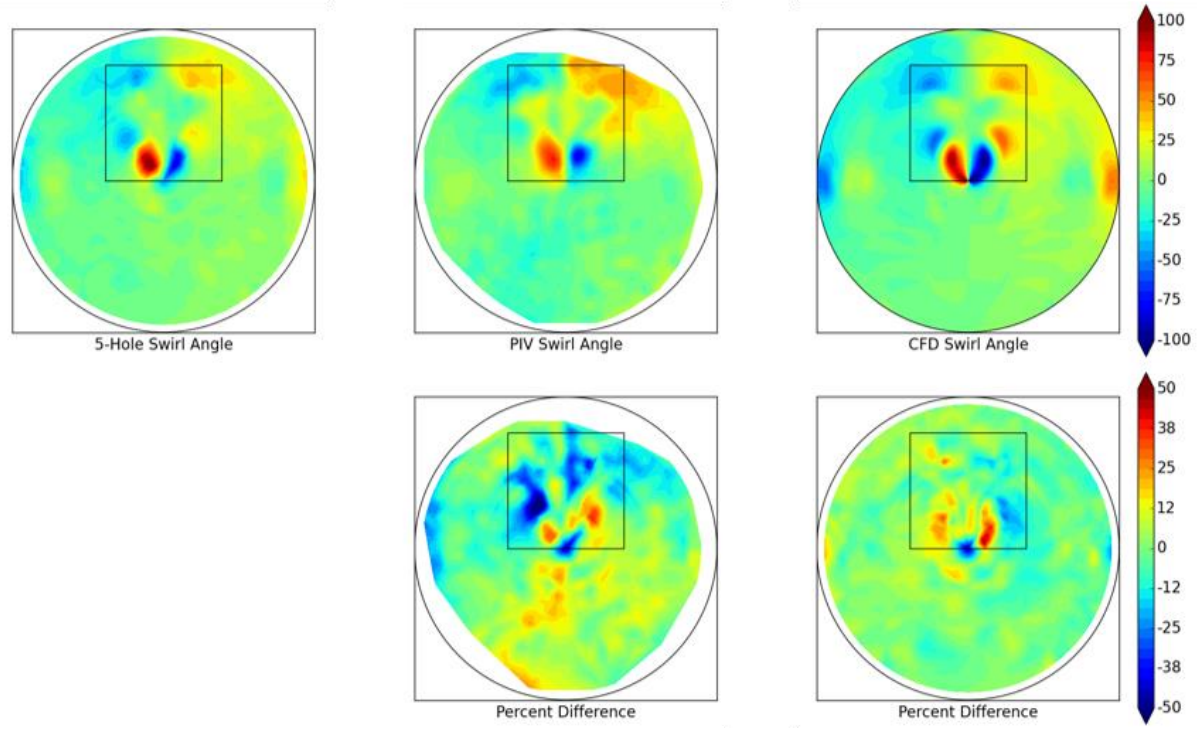


**Figure 20. Subtraction of PIV and CFD swirl angle from the 5-hole data.**

The details of the swirl field show that the swirling flow features of interest are positioned consistently within the AIP. The boxed region from Fig. 21 is zoomed and shown in Fig. 21 with a grid based on fractional span for feature identification. The contour lines for the corresponding swirl flowfield are also shown so that the differences may be identified relative to the flow feature locations. The radial extent of the small swirling flow regions bounded by the box is approximately 75% of span. Two distinct pairs of swirling flow are seen. The first pair is centered approximately 25% from the center on the ordinate with each center of swirl located approximately 20% from the center on the abscissa. The second pair is directly above the first, centered at approximately 60% on the ordinate. The positions of the swirling flow features are quite consistent, indicating consistent generation and propagation of the features.

The difference in the shape and strength of the swirling flow features is most substantial in the region of the strongest swirl. The percent difference contours in Fig. 21 clearly show that the peak differences are located below 35% span, corresponding with the regions of strongest swirl in the flowfield contours. The percent difference for the PIV shows several regions of larger difference, in excess of ±30%, at the edges of the peak swirl regions. The shape and position of the differences indicate strongly a small shift in the position of the swirling flow centers. Such a shift in the position could be explained by the manufacturing tolerances between the 17" and 6" StreamVanes. Due to the scale of the 6" StreamVane, the exit flowfield is very sensitive to small variations in vane geometry. The small shift in position is unimportant relative to capturing the formation and shape of the swirling flow features. The percent difference for the CFD also shows a strong difference along the outside of the peak swirl regions. Some of the difference is due to the symmetry of the CFD flowfield, the remainder is due to the smooth shape of the flow features produced by the RANS simulation. Thus the peak differences in the PIV and CFD relative to the 5-hole measurements are located around the peak swirl regions and do not reduce the effectiveness of either method to capture the flowfield.

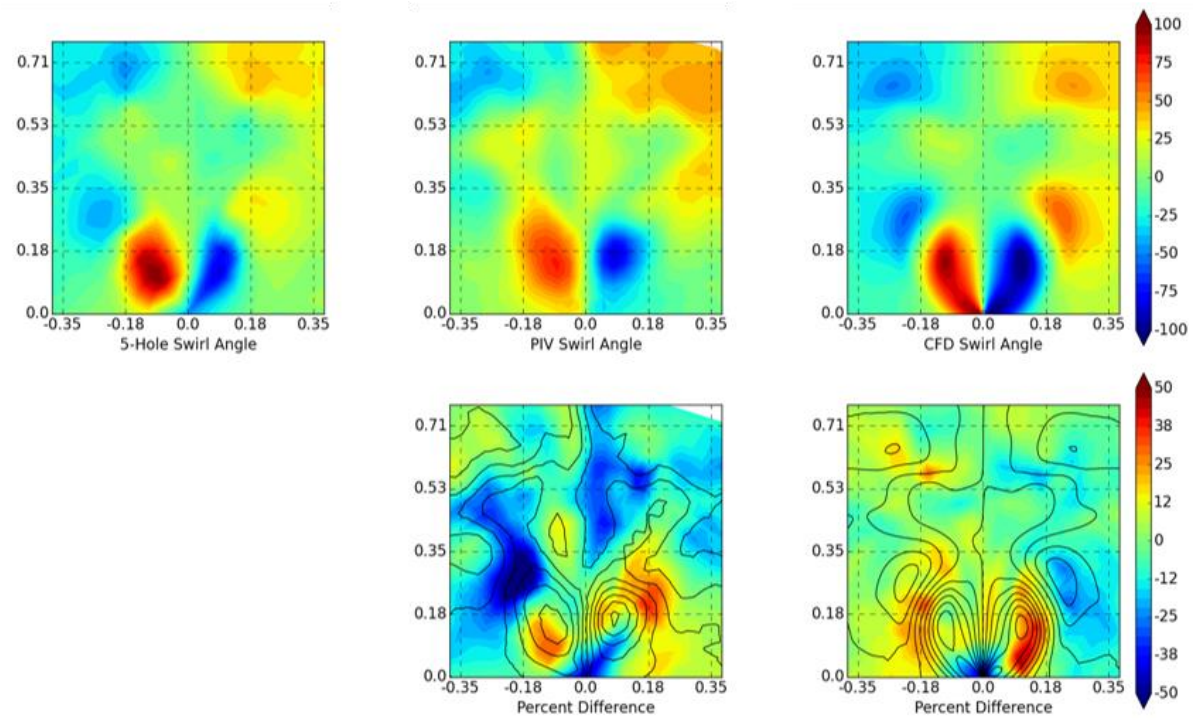


**Figure 21. Details of the subtraction of PIV and CFD swirl angle from the 5-hole data.**

Line plots were used in addition to swirl contours to determine the locations of differences in the swirl angle. Line plots provide quantitative information about the flowfield with specific focus on the difference in magnitude and extent of swirling features.

Constant radius slices were extracted to better understand the discrepancies observed in the percent difference calculation. The ability of the subscale PIV to predict important swirling flow must be judged based upon capture of gross flow features rather than quantitative prediction. The normalized swirl angle for the higher Mach number case is plotted versus circumferential position in Figs. 22 and 23. Each figure shows the 5-hole data, the PIV data taken at the lower Mach number, and the CFD results. The PIV data is accompanied by a dashed line indicating a Clough-Tocher interpolation to densify the display.

A lower radius, r/R = 0.2, was selected first to assess the differences seen near the first ordinate axis gridline in Fig. 21. The circumferential extent of the peak swirl regions was similar but the 5-hole data was offset toward the positive swirl peak (counter-clockwise) relative to the symmetric CFD pattern. The swirl angle for the 5-hole and PIV measurements is also asymmetric in extrema. The asymmetry further accounts for the percent difference peaks and positions seen between the 5-hole and the CFD datasets on the clockwise side of TDC.

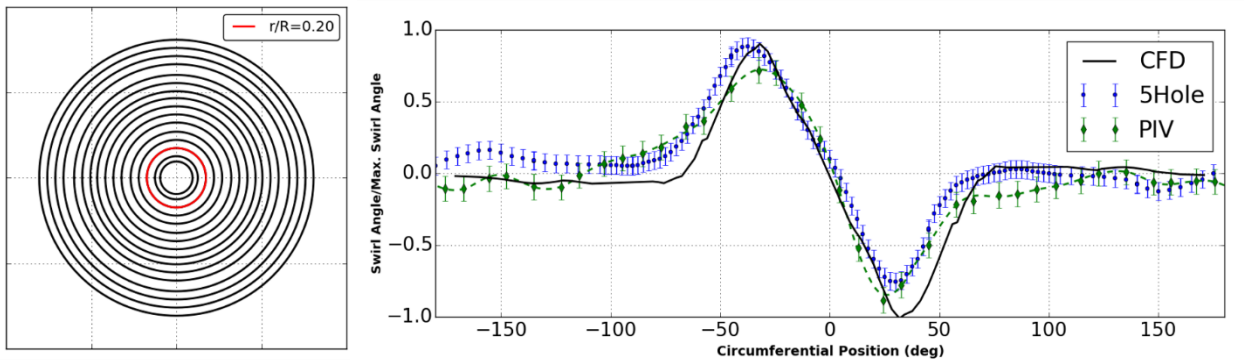


**Figure 22. Circumferential distribution of swirl angle at r/R ≈ 0.20.**

A higher radius, r/R = 0.71, shown in Fig. 23 was selected to analyze the differences in the upper region of the swirling flow. The match between the different methods is acceptable qualitatively, with all three datasets showing

the same overall trends as shown in Fig. 23. The match is also acceptable quantitatively, with error much lower than in the stronger swirling region at lower radius as evident from the close match in peak locations and the low percent difference values in the contours (see Fig. 22).

The quality of the swirl angle match between the 5-hole probe, subscale PIV, and the CFD datasets indicates that Mach number and scaling effects are not substantial for the flowfield generated by the StreamVane. The assertion that swirl angle is insensitive to Mach number is consistent with Fig. 17. The assertion is also analogous to prior investigations by Pazur and Fottner where swirl angle produced by a delta wing was insensitive to changes in corrected speed of a downstream engine (see Ref. 19, Fig. 5).

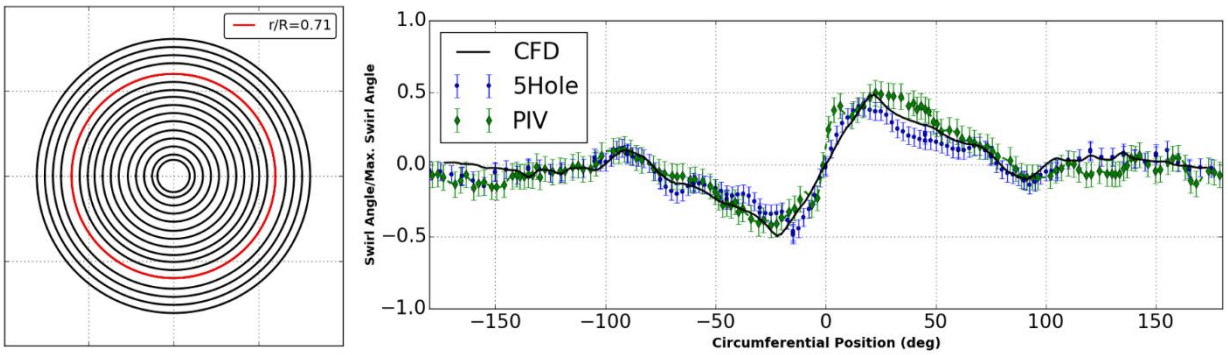


**Figure 23. Circumferential distribution of swirl angle at r/R ≈ 0.71.**

Further assessment of the ability of the CFD method to capture the 5-hole behavior was conducted since CFD simulation is a predominant method for predicting flow around complex geometries. The subtraction technique was again used to assess the ability of CFD to capture the total pressure field variations. The StreamVane was designed to have minimal losses. However, the presence of struts and turning vanes result in wakes. The consistent position and depth of total pressure deficit wake structures further validates the CFD simulation and proves the utility of the CFD method.

The total pressure computed by the CFD was compared to the 5-hole data. The contours and percent difference are shown in Fig. 24 along with a zoom of the region of interest. The CFD grid density is much higher than that of the experimental data points, and the RANS simulation does not properly capture the mixing between the wakes and the core flow due to turbulent mixing. Thus the primary difference between the datasets is the definition and fidelity of the StreamVane wakes. All of the high percent differences are located in positions where the StreamVane wakes are sharply defined in the CFD. All of the high negative percent differences are located in regions where the CFD shows sharp definition of core flow values. Clear flow features associated with the peak swirl regions are shown in the zoomed contour plots with the CFD mimicking the structures seen in the 5-hole data. The CFD captures the total pressure field's flow structures but the solution has sharper defined features than the 5-hole data.

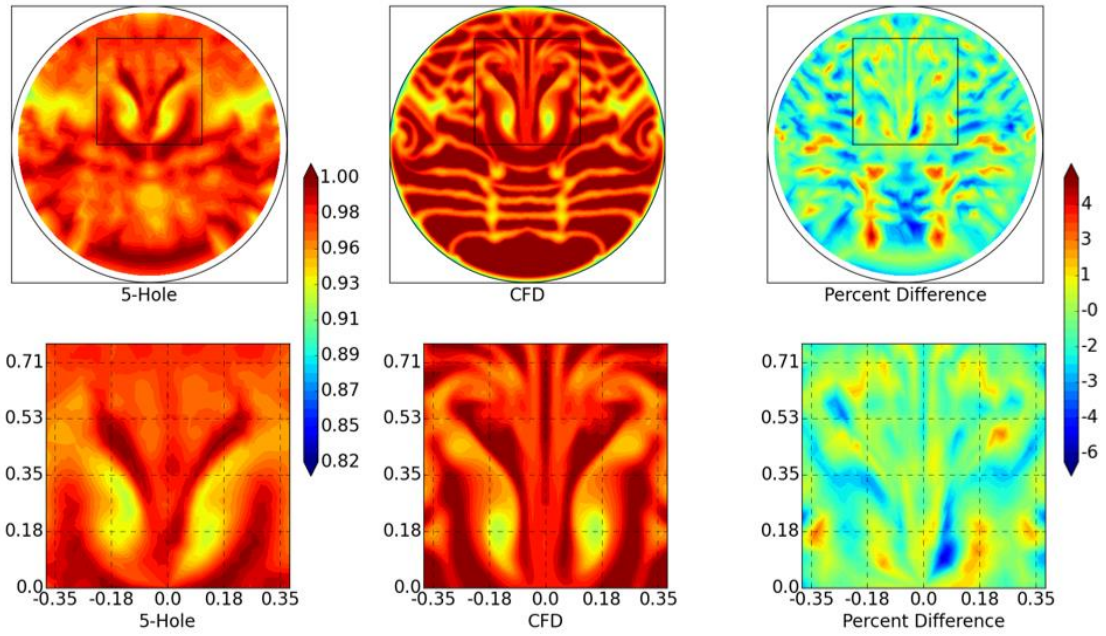


**Figure 24. Subtraction of CFD total pressure from the 5-hole data.**

Comparison of the PIV and CFD to the 5-hole probe data demonstrated the ability to capture the flowfield. The assessment indicated that the CFD was able to capture the total pressure and swirl flowfield. The PIV experiment, despite being subscale and collected at a different Mach number, was able to capture the same flow features adequately in terms of extent and magnitude.

## VI. Conclusion

Subscale PIV and CFD analysis were demonstrated to be effective in characterizing swirling flow downstream of a StreamVane swirl pattern generation system. The success of the PIV and CFD evaluations was based upon comparison to an independent 5-hole probe measurement with direct comparison of flow angles and bulk swirling flow features.

A StreamVane produces swirling flow features with a minimal total pressure distortion to simulate isolated flow angularity seen in existing and future engine installations. The total pressure recovery of the StreamVane was high and the total pressure distortion was limited to wake structures from the StreamVane. Thus the StreamVane can be used to isolate the swirl distortion effects from the total pressure distortion.

Comparisons show that the swirl angle was similar between the CFD and experimental results. The positions of the swirling flow features were consistent between the three methods though magnitudes varied in regions of high swirl.

The swirl flowfield was shown to have little variation with changing Mach number over the tested Mach number range, allowing low Mach number testing of StreamVanes a viable method to confirm the flowfield predicted by CFD. The 5-hole probe data compared well in terms of feature presence, position, and swirl magnitude over the flowfield, and the subscale PIV was able to capture the same structures and positions. Thus the subscale testing at a reduced Mach number will produce a relevant flowfield for validation of CFD predictions.

The subscale PIV testing used reduced resolution of the flowfield to capture the full swirling flow pattern with a single test. The reduced resolution means smaller flow features may not be captured. However, the PIV demonstrated the ability to capture all of the flow features seen in the 5-hole probe measurements and CFD. A single test makes experimental validation with the subscale PIV a cost effective way to assess the performance of a StreamVane.

The ability to isolate the influence of flow angularity on engine systems is crucial in developing design guidance for future integrated propulsion systems. The new approach to swirl pattern generation based on StreamVane technology enables the assessment of swirling flowfields at a reduced cost relative to full system testing.

# Appendix

## A. Subscale StreamVane™ Time-Averaged 3-D PIV Error Analysis

To perform a cursory investigation of the errors in the experimental procedure, two common datasets were obtained one duct diameter downstream of the exit of the StreamVane. The datasets were acquired on two different days, and the PIV set-up was altered for other data acquisition configurations during that time. The results of the comparison provide some insight into the errors present in the PIV data presented. However, since only two common data sets were obtained the full extent of the experimental error cannot be defined.

Due to the large number of images used to compute the average, the error of the mean values is extremely small. This comparison is provided in an attempt to evaluate the errors of the experimental set-up driven by the wind tunnel, laser positioning, PIV calibration, and installation of the StreamVane and downstream duct.

The regions of greatest variation in swirl within the 6" diameter duct are outlined by the white box in Fig. A1. The figure shows the contours of swirl difference between two common PIV experiments at Mach 0.15 located at one duct diameter downstream of the StreamVane exit. This region highlighted in Fig. A1 is also the region where the greatest variation in radial angle was present. This region is explored in detail in Fig. A2 which shows the in-plane velocity field vectors for each of the two cases overlaid onto the contours of differences in swirl between the data sets. In addition, the centers of four individual vortices are identified as numbers 1 through 4. The figure suggests that the relative position of the four vortices are repeated in both data sets. Table 1 outlines the position of each vortex for each of the two repeatability cases in polar coordinates. The table shows that the maximum variation in circumferential position is 3 degrees for vortex number 1, and radially they agree within an average of 2.6% of the span.

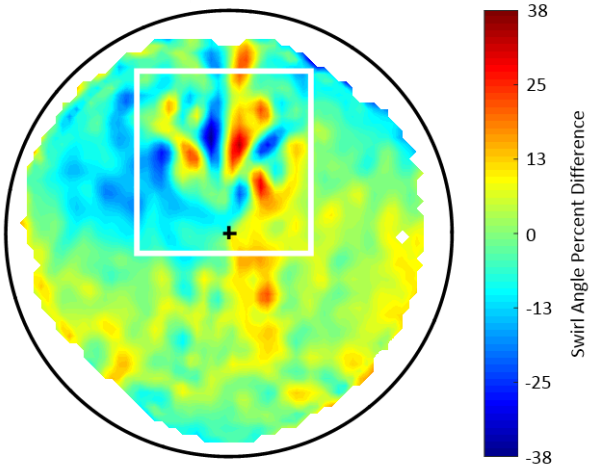


**Figure A1. Swirl Angle Variation (looking downstream).**

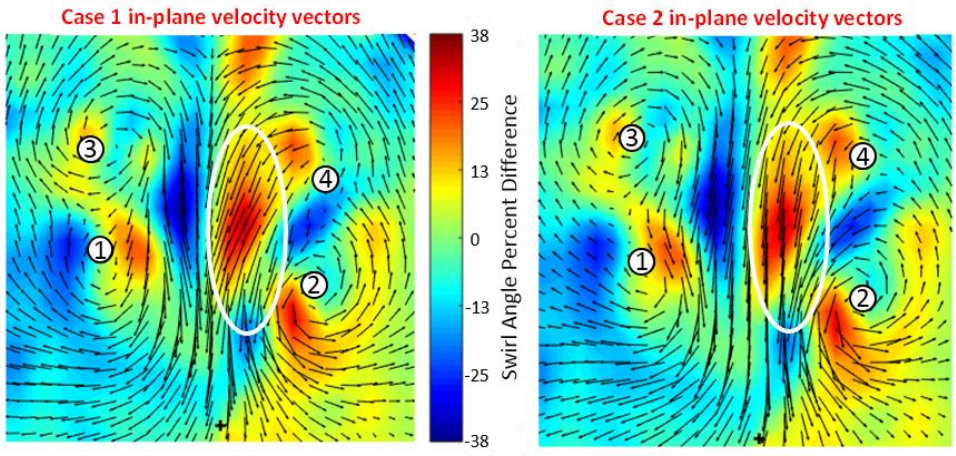


**Figure A2. Details of Variations Between Repeat Data Sets.**

**Table A1. Comparison of Vortex Positions between Case 1 and Case 2**

| Location | % Span (Case 1) | Θ (Case 1) | % Span (Case 2) | Θ (Case 2) | Δ % Span | Δθ |
|---|---|---|---|---|---|---|
| 1 | 42.0 | -35.2 | 39.2 | -32.2 | 2.8 | -3.0 |
| 2 | 32.2 | 34.7 | 34.0 | 37.1 | -1.8 | -2.4 |
| 3 | 60.0 | -23.2 | 60.4 | -23.1 | -0.4 | -0.1 |
| 4 | 50.8 | 23.5 | 56.4 | 21.6 | -5.6 | 1.9 |

The primary driver for the variations in swirl seen can be seen in Fig. A2 by the change in direction of the vector field annotated with a white oval. At the annotated location, the flowfield appears to take a less radial and more circumferential flow direction for case 1 than for case 2. The amount of tangential flow was driven by the position of vortex 2 relative to vortex 4. In case 1 they are closer resulting in more swirl, while in case 2 they are far enough apart to enable more significant radial flow. The differences between the cases represented in Fig. A2 would suggest that the interaction of the four individual vortices results in a slightly different flowfield for the two cases, and therefore the reported swirl angle variations are greater than all other regions of the flowfield. These differences could be a result of small errors in positioning of the PIV laser sheet between the two experiments. The laser was positioned based on markings on the duct, which could result in ±3mm of error in positioning (the laser sheet thickness). It is possible that in these regions – where the vortices are interacting in close proximity to one another – that gradients in the axial direction could be high and therefore axial positioning would be critical. More precise positioning of the laser sheet may reduce these regions of measurement variability.



## Acknowledgments

The authors would like to acknowledge the support from the DoD High Performance Computing Modernization Program in the form of computational hours, software licenses, and data storage.

The authors would also like to acknowledge the research team at the Virginia Tech Turbomachinery and Propulsion Lab for their support in the subscale StreamVane evaluation. Special thanks goes to Tamara Guimarães for her expertise and guidance in acquiring the PIV data presented here and to Professor Walter F. O'Brien (ME) and Professor K. Todd Lowe (AOE) for sponsoring Dr. Copenhaver at Virginia Tech as part of the AFOSR Visiting Scientist Program to conduct the 6" PIV experiments.

## References

[1]Amundson, M., Holm, R., "Distortion Test Capabilities for Future Fighter Aircraft Engines," *25th Joint Propulsion Conference*, AIAA-89-2946, Monterey, CA, 1989.

[2]Brossman, J., Ball, P., Smith, N., Key, N., "Sensitivity of Multistage Compressor Performance to Inlet Boundary Conditions," *AIAA Journal of Propulsion and Power*, Vol. 30, No. 2, 2014.

[3]King, R.W., Neuman, H.E., "A Method of Distortion Pattern Synthesis for High Response Data Screening," *12th Propulsion Conference*, AIAA-76-704, Palo Alto, CA, 1976.

[4]Hoopes, K.M., O'Brien, W.F., "The StreamVane Method: A New Way to Generate Swirl Distortion for Jet Engine Research," *49th AIAA/ASME/SAE/ASEE Joint Propulsion Conference*, AIAA 2013-3665, San Jose, CA, 2013.

[5]Guimarães, T., Lowe, K.T., Nelson, M., O'Brien, W.F., Kirk, C., "Stereoscopic PIV Measurement in a Turbofan Engine Inlet with Tailored Swirl Distortion," *31st AIAA Aerodynamic Measurement Technology and Ground Testing Conference*, AIAA-2015-2866, Dallas, TX, 2015.

[6]Dunavant, J.C., "Cascade Investigation of a Related Series of 6-Percent-Thick Guide-Vane Profiles and Design Charts," NACA TN 3959, 1957.

[7]Lieblein, S., and Sandercock, D. M., "Compressibility Correction for Turning Angles of Axial-Flow Inlet Guide Vanes," NACA TN 2215, 1950.

[8]Hoopes, K.M., "A New Method for Generating Swirl Inlet Distortion for Jet Engine Research," MS Thesis, Virginia Polytechnic Inst. and State Univ., Blacksburg, VA, 2013.

[9]StarCCM+, Software Package Manual, Version 10.04, CD-adapco, Melville, NY, 2015.

[10]Menter, F. R., "Two-Equation Eddy-Viscosity Turbulence Models for Engineering Applications", *AIAA Journal*, Vol. 32, No. 8, 1994, pp. 1598-1605.

[11]Description of AFRL exhauster capability, http://www.wpafb.af.mil/shared/media/document/AFD-070425 062.pdf

[12]SAE S-16 Committee, "Gas Turbine Engine Inlet Flow Distortion Guidelines," ARP 1420, Society of Automotive Engineers, 1998.

[13]Lee, C.S, and Wood, N.J., "Calibration and Data Reduction for a Five-Hole Probe," Joint Institute for Aeronautics and Acoustics, Stanford University, JIAA TR-73, 1986.

[14]Paul, A.R., Upadhyay, R.R., Jain, A., "A novel calibration algorithm for five-hole pressure probe," *International Journal of Engineering, Science and Technology*, Vol. 3, No. 2, 2011, pp. 89-95.

[15]Tkacik, P,T., "Cascade Performance of Double Circular Arc Compressor Blades at High Angles of Attack," MS Thesis, Virginia Polytechnic Inst. and State Univ., Blacksburg, VA, 1982.

[16]Yocum, A.M, "An Experimental and Numerical Investigation of the Performance of Compressor Cascades with Stalled Flow," PhD Dissertation, Mechanical Engineering Dept., Virginia Polytechnic Inst. and State Univ., Blacksburg, VA, 1988.

[17]Raffel, M., Willert, C.E., and Kompenhans, J., *Particle Image Velocimetry: A Practical Guide*, Springer Berlin Heidelberg, 1998.

[18]Alfeld, P., "A Trivariate Clough-Tocher scheme for Tetrahedral Data," *Computer Aided Geometric Design*, Vol. 1, No. 2, 1984, pp. 169-181.

[19]Pazur, W., and Fottner, L., "The Influence of Inlet Swirl Distortions on the Performance of a Jet Propulsion Two-Stage Axial Compressor," *Journal of Turbomachinery*, Vol. 113, 1991, pp. 233-240.